Measurement of electrotransport induced excess vacancies in silver

1998 J. Phys.: Condens. Matter 10 2901

(http://iopscience.iop.org/0953-8984/10/13/009)

J. Phys.: Condens. Matter **10** (1998) 2901–2914. Printed in the UK PII: S0953-8984(98)85173-4

Measurement of electrotransport induced excess vacancies in silver

Jürgen Ruth†

Institut für Metallphysik, Universität Göttingen, D-37073 Göttingen, Hospitalstraße 3–7, Germany

Received 13 June 1997, in final form 11 December 1997

Abstract. The mean free path of excess vacancies that are generated during electromigration in silver has been determined employing a combined electromigration diffusion technique. The method is based on the assumption that during electromigration a steady-state excess vacancy distribution exists. The latter is determined by a measurement of diffusion enhancements of copper in silver at different positions along the electric field gradient. Under certain conditions that are expected to be fulfilled in our experiments an evaluation of the measured diffusion enhancements by means of the steady-state theory yields the mean square free paths of the excess vacancies. They are found to be between 1.6×10^{-4} and 5.4×10^{-4} cm^2.

1. Introduction

It is well known that electromigration and thermotransport in metallic systems are associated with a flow of vacancies. During electrotransport experiments in isothermal systems a steady state excess vacancy distribution is expected to be developed that depends on the experimental parameters such as temperature and the electrical field gradient, the physical properties of the system and on the mean free path of the vacancies in the considered system. Hence, the latter could be determined if excess vacancy concentrations could be measured. In the present paper a method is employed that allows us to measure excess vacancy concentrations if certain limiting conditions are fulfilled. This method is based on measurements of diffusion flows perpendicular to applied electric field gradients. The method applies also to thermotransport induced deviations of vacancy concentrations from equilibrium and was first described by Hehenkamp [1].

2. Theory

2.1. Electromigration induced excess vacancy concentrations

As for any non-conserved species, the local rate of change of vacancy concentrations is given by

$$\frac{\partial C_V}{\partial t} = -\boldsymbol{\nabla} \cdot \boldsymbol{J}_V + R_V \tag{1}$$

† Present address to which correspondence should be directed: Jürgen Ruth, c/o Gunther Ruth, Alsumer Straße 32, 27632 Dorum, Germany.

0953-8984/98/132901+14$19.50

if the number of lattice sites remains constant during the processes of diffusion and electromigration. R_V is the local creation or annihilation rate of vacancies. It is well known that electromigration is associated with a flux of vacancies $\boldsymbol{J}_V^{eq.}$ that in turn gives rise to the development of local vacancy concentration gradients. Hence, the total flux of vacancies is given by

$$\boldsymbol{J}_V = -D_V \boldsymbol{\nabla} C_V + \boldsymbol{J}_V^{eq.} \tag{2}$$

with the vacancy diffusion coefficient D_V. The electromigration induced flux of vacancies is

$$\boldsymbol{J}_V^{eq.} = \boldsymbol{v} C_V \tag{3}$$

where $\boldsymbol{v}$ is the velocity of a vacancy that it attains under exertion of an electric field E. With the mobility of the vacancies

$$u_V = \frac{\boldsymbol{v}}{\boldsymbol{E}} \tag{4}$$

and the Nernst–Einstein equation as applied to driving forces due to an electric field

$$\frac{u_V}{D_V} = \frac{Z^* e}{kT} \tag{5}$$

$\boldsymbol{J}_V^{eq.}$ becomes

$$\boldsymbol{J}_V^{eq.} = \frac{D_V E Z^* e}{kT} C_V. \tag{6}$$

Z^* is the effective valence of a vacancy and e the charge of an electron. For small deviations of the vacancy concentrations C_V from the equilibrium concentration $C_V^{eq.}$ it is justified to assume non-saturable sources or sinks of vacancies, for which the creation or annihilation rate becomes

$$R_V = \frac{C_V^{eq.} - C_V}{\tau_V}. \tag{7}$$

τ_V is the mean lifetime of a vacancy. For larger deviations of C_V from the equilibrium vacancy concentration R_V is determined by the chemical potential of the vacancies that are considered to form an ideal solution in the host metal:

$$\mu_V = kT \ln \frac{C_V}{C_V^{eq.}} \tag{8}$$

which again can be approximated mathematically for smaller deviations by

$$\mu_V = kT \left(\frac{C_V - C_V^{eq.}}{C_V^{eq.}} \right). \tag{9}$$

Hence, in general equation (7) has to be replaced by

$$R_V = -\alpha \frac{\mu_V}{kT} \tag{10}$$

with

$$\alpha = \frac{C_V^{eq.}}{\tau_V}. \tag{11}$$

Combining equations (1) to (7) yields

$$\frac{\partial C_V}{\partial t} = D_V \Delta C_V - Z^* e \boldsymbol{E} \cdot \frac{D_V}{kT} \boldsymbol{\nabla} C_V + \frac{C_V^{eq.} - C_V}{\tau_V}. \tag{12}$$

If the sources and sinks of vacancies are sufficiently abundant and efficient a steady state of local vacancy concentrations

$$\frac{\partial C_V}{\partial t} = 0 \tag{13}$$

can be assumed to prevail. With the definition of vacancy supersaturation by the normalized excess vacancy concentration

$$C_V^{exc.} = \frac{C_V}{C_V^{eq.}} \tag{14}$$

and with the abbreviations

$$\boldsymbol{A} = \frac{Z^* e E}{kT} \tag{15a}$$

and

$$B = \frac{1}{D_V \tau_V} \tag{15b}$$

equation (12) leads for the steady-state case to the differential equation

$$\Delta C_V^{exc.} - \boldsymbol{A}\boldsymbol{\nabla} C_V^{exc.} - B(C_V^{exc.} - 1) = 0. \tag{16}$$

Via the Einstein relation

$$\langle x_V^2 \rangle = 6 D_V \tau_V \tag{17}$$

the parameter B is directly related to the mean square free path of a vacancy $\langle x_V^2 \rangle$. With the boundary conditions $\boldsymbol{J}_V = \boldsymbol{0}$ being fulfilled for $x = \pm L/2$ (where L is the axial length of the specimen) a solution of equation (16) yields the steady-state distribution of relative excess vacancy concentrations

$$C_V^{exc.} = 1 + C_1 \exp(r_1 x) + C_2 \exp(r_2 x) \tag{18}$$

with the parameters

$$r_{1,2} = \frac{A}{2} \pm \left[\left(\frac{A}{2} \right)^2 + B \right]^{1/2} \tag{19a}$$

$$C_1 = A \frac{\sinh(r_2 L/2)}{r_2 \sinh[(r_1 - r_2)L/2]} \tag{19b}$$

and

$$C_2 = A \frac{\sinh(r_1 L/2)}{r_1 \sinh[(r_2 - r_1)L/2]}. \tag{19c}$$

Details of the calculations are given in appendix A. In our experiments fulfillment of the above-mentioned boundary condition has been realized by coating both ends of the sample with a tungsten layer. If, however, the boundary condition $\boldsymbol{J}_V = \boldsymbol{0}$ should not be fulfilled at the ends of the specimen, the parameters C_1 and C_2 have to be replaced by the expressions

$$C_1' = \frac{A_{cat}' \exp(r_2 L/2) - A_{an}' \exp(-r_2 L/2)}{2 r_2 \sinh[(r_1 - r_2)L/2]} \tag{20a}$$

and

$$C_2' = \frac{A_{cat}' \exp(r_1 L/2) - A_{an}' \exp(-r_1 L/2)}{2 r_1 \sinh[(r_1 - r_2)L/2]} \tag{20b}$$

with

$$A'_{cat} = A - \frac{J_V^{cat}}{D_V C_V^{eq}} \tag{21a}$$

and

$$A'_{an} = A - \frac{J_V^{an}}{D_V C_V^{eq}} \tag{21b}$$

where J_V^{cat} and J_V^{an} are the steady-state vacancy fluxes at the cathodic and the anodic ends of the specimen, respectively. From equation (19*a*) follows that $r_1 > 0$, $r_2 < 0$ and $(r_1 - r_2) > 0$. Hence, equations (19*b*) and (19*c*) can be rewritten as

$$C_1 = -A\frac{\sinh(-r_2 L/2)}{r_2 \sinh[(r_1 - r_2)L/2]} \tag{22a}$$

and

$$C_2 = -A\frac{\sinh(r_1 L/2)}{r_1 \sinh[(r_1 - r_2)L/2]}. \tag{22b}$$

If the condition

$$\left(\frac{A}{2}\right)^2 \ll B \tag{23}$$

is sufficiently fulfilled, the functions $\sinh(\varphi)$ can be approximated by exponential functions. As discussed in appendix 2, this condition is fulfilled in all cases physically conceivable here. Hence, we obtain

$$C_1 = -\frac{A}{r_2} \exp\left(-r_1 \frac{L}{2}\right) \tag{24a}$$

and

$$C_2 = -\frac{A}{r_1} \exp\left(r_2 \frac{L}{2}\right). \tag{24b}$$

For the case of non-vanishing vacancy fluxes at the cathodic and anodic ends of the specimen these parameters are given by the expressions

$$C'_1 = -\frac{A'_{an}}{r_2} \exp(-r_1 L/2) \tag{25a}$$

and

$$C'_2 = -\frac{A'_{cat}}{r_1} \exp(r_2 L/2). \tag{25b}$$

Inserting the expressions (24*a*) and (24*b*) into equation (18) leads to the excess vacancy contribution

$$(C_V^{exc.} - 1) = -\frac{A}{r_2} \exp\left(-r_1\left(\frac{L}{2} - x\right)\right) - \frac{A}{r_1} \exp\left(r_2\left(\frac{L}{2} + x\right)\right). \tag{26}$$

If, surpassing condition (23), the stronger condition

$$\frac{A}{2} \ll B^{1/2} \tag{27}$$

is fulfilled, equation (19*a*) can be approximated by

$$r_{1,2} = \pm B^{1/2} \tag{28}$$

and equation (26) becomes

$$(C_V^{exc.} - 1) \cong \frac{A}{B^{1/2}} \exp\left(-\frac{B^{1/2}L}{2}\right)\left[\exp\left(B^{1/2}x\right) - \exp\left(-B^{1/2}x\right)\right]. \tag{29}$$

In this case and for sufficiently large values of x, i.e.

$$x \gg \sqrt{\langle x_V^2 \rangle / 6} \tag{30}$$

the second term in the square brackets can be neglected yielding

$$\ln(C_V^{exc.} - 1) \cong G + B^{1/2}x \tag{31}$$

with

$$G = \ln\left(\frac{A}{B^{1/2}}\right) - B^{1/2}\frac{L}{2} \tag{32}$$

or, for non-vanishing vacancy fluxes at the ends of the specimen,

$$G' = \ln\left(\frac{A'_{an}}{B^{1/2}}\right) - B^{1/2}\frac{L}{2}. \tag{33}$$

The slope of a logarithmic plot of otherwise measured values of $(C_V^{exc.} - 1)$ versus x should yield the mean square free path of a vacancy. Note that in any case one has to make sure that the linear relation (31) holds for larger values of x (condition (30)) and that the determined value of B fulfills the condition (27). But, according to equations (31) to (33), the slope of the logarithmic plot is not affected by possible non-vanishing vacancy fluxes at the cathodic and anodic ends of the specimen. Also, as shown in appendix B, for many cases the occurrence of these fluxes can be neglected.

2.2. Diffusion enhancement by excess vacancies

The enhancement of diffusion by excess vacancies is defined by the ratio $D_i/D_i^{eq.}$. D_i is the diffusion coefficient of component i in a dilute solid solution at the actual excess vacancy concentration and $D_i^{eq.}$ that one obtained at equilibrium vacancy concentration. The local diffusivity of any component in an alloy is proportional to the local vacancy concentration C_V:

$$D_i = \gamma f_i \Gamma_i C_V \tag{34}$$

where γ is a steric factor, depending on the structure of the alloy, f_i the diffusional correlation factor of component i in the alloy and Γ_i the jump rate of i atoms into adjacent vacant lattice sites. Since in diluted alloys γ, f_i as well as Γ_i do not depend on the local vacancy concentration, the ratio of the diffusivities as obtained at equilibrium, $C_V^{eq.}$, and at locally higher vacancy concentrations, C_V, becomes

$$\frac{D_i}{D_i^{eq.}} = \frac{C_V}{C_V^{eq.}} = C_V^{exc.}. \tag{35}$$

3. Experimental procedure

A combination of equations (31) and (35) allows us to determine the mean square free path of a vacancy $\langle x_V^2 \rangle$ from the slope of a plot of $\ln((D_i/D_i^{eq.}) - 1)$ versus x according to the equation

$$\ln\left(\frac{D_i}{D_i^{eq.}} - 1\right) \cong G + \frac{\sqrt{6}}{\sqrt{\langle x_V^2 \rangle}}x. \tag{36}$$

For a measurement of the local diffusivities D_i the method of lateral isothermal diffusion during electromigration has been employed, whereas the equilibrium diffusivities may be obtained either from independently performed tracer diffusion experiments or by an evaluation of the diffusional penetration at about $x = 0$, a region where diffusion is expected to remain uneffected by electromigration. For practical use it is convenient to employ an x-coordinate that is defined by the distance x^T from the cathode that can easily be transformed to the x-coordinate used in equation (36) by the relation

$$x^T = \frac{L}{2} - x. \tag{37}$$

In the following, the preparation techniques, the combined electrotransport and diffusion apparatus and the methods of determination of the pertinent diffusion coefficient are described.

3.1. Preparation of specimens

As starting material for the specimens silver rods with a nominal purity of 99.999at.%, from Demetron Hanau, have been utilized. The prepared cylinder shape specimens had a diameter of approximately 6 mm and a length of 5 mm. A radial hole had been eroded sidewise into the cylinder for the thermocouple to be used during the experiments, figure 1.

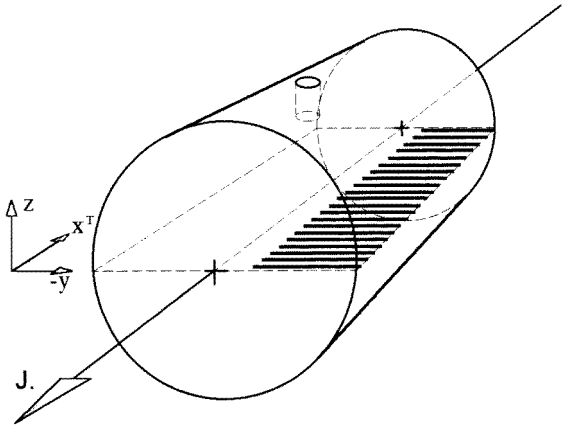

Figure 1. Schematic representation of the silver specimen. The bold lines in y-direction represent the quantitative penetration curves as obtained for different positions along the longitudinal axis. The specimen was cut by spark erosion in the x^T, y-plane (see dashed line).

In order to remove sulphide layers, that are almost unavoidable at silver surfaces, the specimens had been polished, etched and subsequently cleaned in an ultrasonic bath of alcohol and acetone. The formation of any new sulphide layers had been prevented by keeping the specimens in an desiccator between further preparation steps and in acetone during such steps. Subsequently, the specimens had been recrystallized in a vacuum chamber at 1023 K for about 24 hours.

Before electrolytical coating of the samples with copper any possible residues of grease had been carefully removed by cleaning in a sodium persulphate solution and subsequently any remaining sodium had been washed off by means of acetone in an ultrasonic bath. The composition of the employed cyanide electrolyte and the preparation parameters for the coating procedure are given in table 1.

Table 1. Compounds of the employed cyanide electrolyte (composition of a 1000 ml solution).

Copper(I) cyanide	CuCN	22.5 g l^{-1}
Sodium cyanide	NaCN	30 g l^{-1} or KCN 39.9 g l^{-1}
Sodium carbonate monohydrate	$Na_2CO_3 \cdot H_2O$	7.5 g l^{-1}
Sodium pyrosulphite	$Na_2S_2O_5$	3.8 g l^{-1}

Using these chemicals we adjusted the pH-value to 11.

Best results of the coating process have been obtained with anodic and cathodic currents of 10 mA for samples with a surface of 1.5 cm^2. Any undesired incorporation of hydrogen in the growing copper layers can best be avoided by employing a bath temperature of 305 to 325 K. With an exposure time of 8 minutes a copper layer with a thickness of (2 ± 0.15) μm had been accomplished. The required homogeneity of the copper layer thickness was achieved by an alternating change of the current direction.

After removal of the copper layers at both front surfaces of the specimens these had been sputtered with tungsten to prevent any axial in- or outflow of vacancies in order to fulfill the boundary condition $\boldsymbol{J}_V = \mathbf{0}$ stated in section 2.1 of this paper.

3.2. The electromigration and diffusion apparatus

A schematic cross-section of the used electromigration and diffusion apparatus is given in figure 2. An axial direct current with a density exceeding 3000 A cm^{-2} gave rise to the electromigration of vacancies as well as to an elevation of the sample temperature to 943 K. The sample temperature could be maintained with an accuracy of ± 1.5 K during the entire duration of the experiment. By means of a jacket heating device (HC) combined with a PID control unit (see figure 2) the difference between the temperatures at the specimen's ends, T_1 and T_2, could be kept as low as 1 K. Thus, any additional thermotransport effects caused by a possible temperature gradient can be excluded.

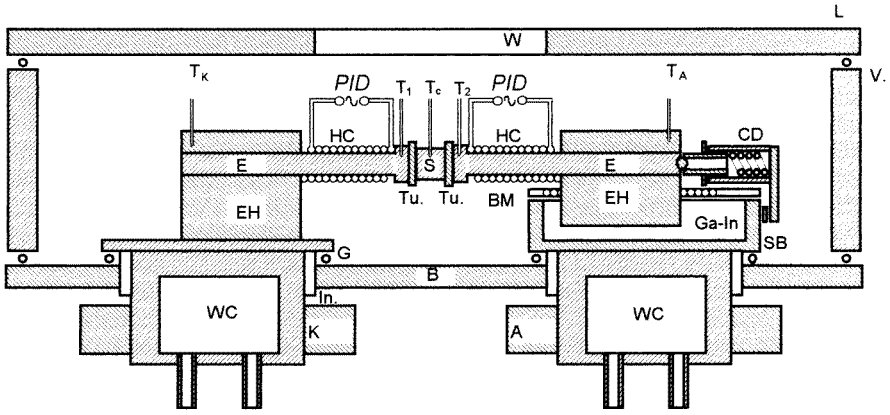

Figure 2. Cross-section of the electromigration and diffusion apparatus. A: current supply (anode). G: gasket. S: specimen. BM: ball mount. Ga–In: gallium–indium bath. SB: stainless steel bath trough. CD: spring (clamping device). HC: jacket heat conductor. Tu.: tungsten foil. B: bottom. In.: insulation V: vacuum chamber (2×10^{-3} Pa). E: electrodes (the anode is movable). K: current supply (cathode). WC: water cooling. EH: electrode holder. L: lid. W: window. PID: proportional (P.) , integrating (I.) and differentiating (D.) control unit. T_A, T_K, T_1, T_2, T_C (control): by means of Ni–CrNi thermocouples (Philips).

An experimental duration of 10 days is required for achieving a sufficiently long steady-state period with negligible incubation time, and a measurable diffusional penetration of the copper into the silver cylinder.

3.3. Measurements of diffusion coefficients

For the diffusion measurements the specimens had first been cut axially by spark erosion; subsequently, the flat surfaces had been polished and concentration penetration curves of the coated copper into the interior of the silver cylinder could be measured at different axial positions x^T. A schematic drawing of the situation is given in figure 1. Concentration penetration curves had been obtained employing a CAMECA SX 50 electron-probe x-ray microanalyser (EPMA). The points of measurement had a distance of approximately 5 μm from each other. The curves had been evaluated by means of the equation

$$C_{Cu}(y,t) = \frac{S_0}{\sqrt{\pi D_{Cu} t}} \exp\left[-\frac{y^2}{4D_{Cu}t}\right] \tag{38}$$

that is appropriate for diffusion in semi-infinite half-systems. Here S_0 is the total amount of incorporated copper per unit area, D_{Cu} the diffusion coefficient of copper (assumed to be concentration independent) and y the coordinate in the diffusion direction; t and C_{Cu} are defined as usual for diffusion experiments. The assumption of a constant diffusion coefficient is justified as long as the condition of dilute solid solution is fulfilled, as is the case in our experiments. The slope of a plot of $\ln(C_{Cu}/C^0_{Cu})$ versus y^2 reveals the diffusion coefficient D^{Ag}_{Cu} for the respective concentration penetration curve. More than 22 curves had been evaluated in this way for each sample. The axial distance of the curves had a distance of 10 μm from each other at the extreme ends of the specimen, increasing step by step toward the middle of the sample to reach ultimately an amount of 500 μm.

3.4. Reference measurements

In order to utilize equation (36) the reference diffusion coefficient $(D^{Ag}_{Cu})^{eq.}$ has to be known for the respective diffusion temperature. We have measured the $(D^{Ag}_{Cu})^{eq.}$ at the temperatures 914.6 and 1011.8 K by means of tracer techniques. The obtained values of the diffusion coefficients are $1002(25) \times 10^{-15}$ and $1130(25) \times 10^{-14}$ m^2 s^{-1}, respectively. The annealing temperature could be maintained constant within an accuracy of 0.25 K. In figure 3 our results are given together with data that had been obtained in earlier works. For the determination of the diffusion enhancement at 943 K, as plotted in figure 4, we have employed a reference diffusion coefficient of 2.12×10^{-15} m^2 s^{-1}. This value is deduced from our reference measurements under the assumption of an Arrhenius type temperature dependence.

For the evaluation of our own reference measurements we excluded near-surface regions where some inhibition of diffusion had been observed.

4. Results and discussion

Measurements have been carried out on three specimens. The experimental parameters are listed in table 2; for all experiments the annealing temperature was 943 K.

As a typical example, the apparent electromigration induced diffusion enhancement $D^{Ag}_{Cu}/(D^{Ag}_{Cu})^{eq.} = C_V^{exc.}$ is plotted versus the axial coordinate x^T for specimen No 1 in figure 4.

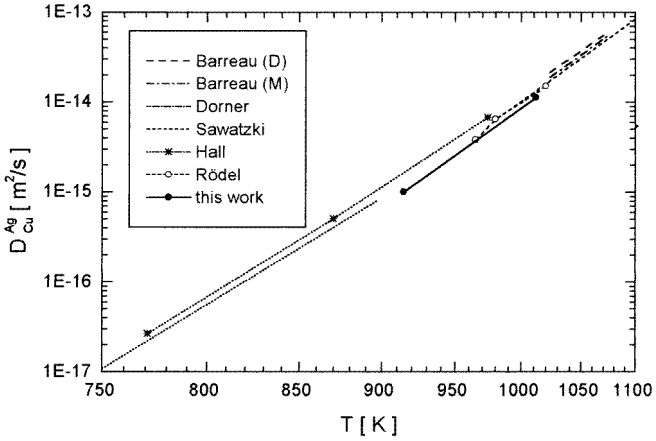

Figure 3. Survey of the diffusion coefficient values as obtained by different authors [2–6] and our data. D refers to an assumption of constant diffusion coefficients, M to employment of the Matano method.

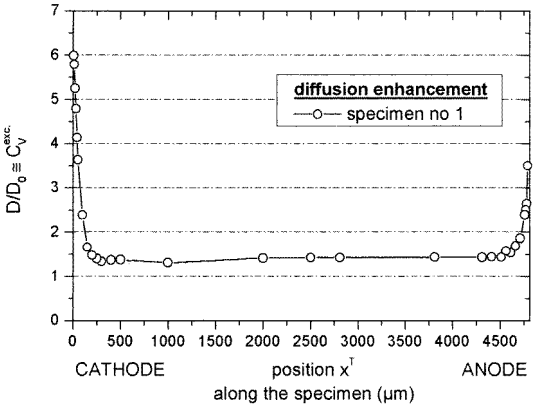

Figure 4. Diffusion enhancement as a function of the distance from the cathode, x^T; specimen No 1.

Table 2. Experimental parameters of our measurements.

Specimen No.	Duration of experiments 10^3 [s]; [d]	Length of specimen [μm]	Current density [A cm^{-2}]	Thickness of copper layer [μm]
1	811 ≈ 9.4	4804	3623	1.66
2	601 ≈ 7.0	4803	3489	1.75
3	883 ≈ 10.2	4469	5024.8	1.78

In all of our three experiments an apparent diffusion enhancement is observed at both ends of the specimen. But, in any case the diffusion enhancement on the cathodic side is much more pronounced than on the anodic side. Furthermore, the apparent diffusion enhancement does not vanish at about the longitudinal centre of the specimen as it should according to the definition of the excess vacancy concentration. However, the latter can

be explained by a deviation of the independently measured equilibrium diffusivities from those prevailing at experimental conditions of the electromigration experiments. Also, it is likely that the actual temperatures at about $x = 0$ did not agree with the diffusion temperatures of the tracer experiments. The phenomenon of an apparent asymmetric diffusion enhancement at the ends of the specimen can be explained by a superposition of two effects: (i) a boundary diffusion effect at both front ends of the specimen and (ii) the effect of electromigration considered here. Obviously, an appreciable boundary diffusion flow of copper occurs between the front ends of the silver specimen and the sputtered tungsten layers. A further penetration of the copper in the axial direction into the silver rod proceeds via volume diffusion. Since the temperatures at both ends of the specimen do not significantly deviate from the temperature as measured at about $x = 0$, the boundary diffusion effect *alone* should yield an equal increase of the copper concentration at both ends of the sample, whereas the electromigration effect *alone* should yield according to equation (29) a symmetric penetration curve with a negative branch at the anodic side of the specimen. From the measured penetration curves the individual contributions of the two effects can therefore be obtained under the only premises that boundary diffusion yields *equal* concentration enhancements on both ends of the sample and electromigration an *S-shape symmetric* concentration penetration curve.

Therefore, we have corrected the measured curves in two steps. Firstly, we have vertically shifted them to touch the $C_V^{exc.} = 1$ line. In all of our experiments this correction corresponds to the assumption of a reference diffusion coefficient of $(D_{Cu}^{Ag})^{eq} \cong 3.3 \times 10^{-15}$ m^2 s^{-1}. This value is in agreement with a value that can be obtained from Hall's measurements for 943 K, figure 3, but it could also be deduced from our measurements of tracer diffusion coefficients if the sample temperature were 10 to 20 K higher than assumed (see figure 3). Subsequently, a subtraction of equal amounts $\Delta C_{corr.}$ from the observed apparent diffusion enhancements at the anodic and cathodic *ends*, $C_{V,an.}^{exc.}$ and $C_{V,cat.}^{exc.}$, yields reduced diffusion enhancements $(C_V^{exc.} - 1)$ of equal amounts but opposite signs at both ends of the specimen. Analogously, a correction of the entire curve has been carried out by pair-wise correcting the measured values corresponding to equal distances from the electrodes. This procedure leads to a symmetric $(C_V^{exc.} - 1)$ curve touching the $(C_V^{exc.} - 1) = 0$ line, figure 5, where the individual $C_V^{exc.}$-values are related to the corresponding measured values

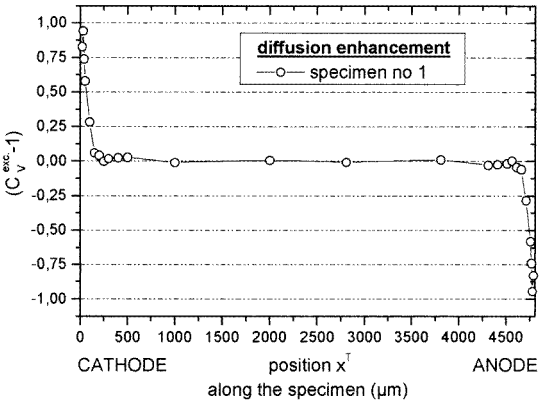

Figure 5. Corrected diffusion enhancement as a function of the distance from the cathode, x^T, according to equation (39); specimen No 1.

on the cathodic and the anodic *sides* of the specimen, $C_V^{exc.}$ and $C_{V,an.}^{exc.}$, via the equation

$$(C_V^{exc.} - 1) = \frac{C_{V,cat.}^{exc.} - C_{V,an}^{exc.}}{2}. \tag{39}$$

For the cathodic half-space of the specimen these values, with their exponential fit function, are replotted in figure 6. When the corrected values of diffusion enhancement are plotted as $\ln(C_V^{exc.} - 1)$ versus x^T one obtains figure 7. This curve can be approximated by a straight line (see linear regression) at larger values of x, which correspond via equation (37) to small values x^T. Analogous curves had been obtained for specimen nos 2 and 3, figures 8 and 9.

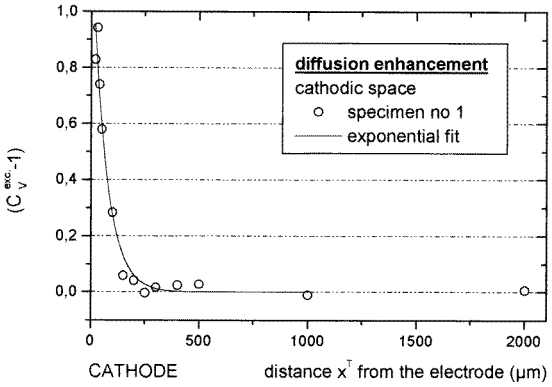

Figure 6. Corrected cathodic space diffusion enhancement as a function of the distance from the cathode, x^T, according to equation (39) with approximated exponential fit; specimen No 1.

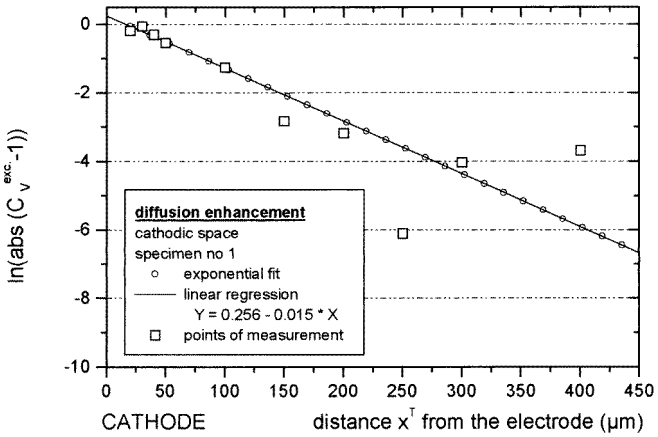

Figure 7. $\ln[\mathrm{abs}(C_V^{exc.} - 1)]$ graph versus x^T corresponding to equation (36). The slope of this plot represents the mean square free path of the vacancies of specimen No 1.

For our three specimens we calculated from the slopes of these curves for the mean square free path $\langle x_V^2 \rangle$ the values 2.5×10^{-4}, 5.4×10^{-4} and 1.6×10^{-4} cm^2 that correspond to mean free path values of excess vacancies of 160, 230, and 125 μm, respectively. It should be noted that with these data the condition (30) is fulfilled for the entire evaluated ranges of figures 7 to 9. With an assumed diffusivity of vacancies $D_V = 1.00 \times 10^{-10}$ m^2 s^{-1} at

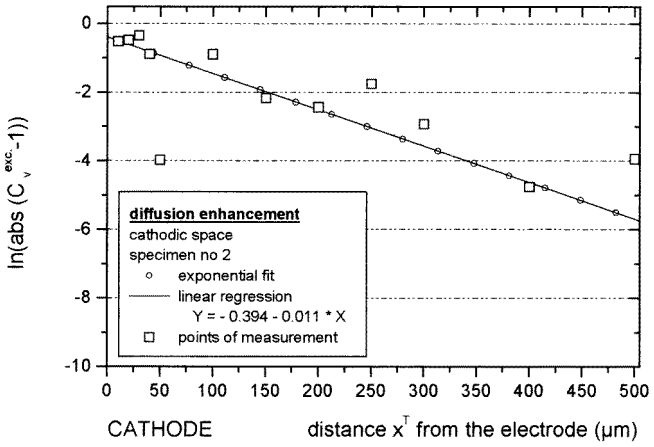

Figure 8. ln[abs($C_V^{exc.} - 1$)] graph versus x^T corresponding to equation (36). The slope of this plot represents the mean square free path of the vacancies of specimen No 2.

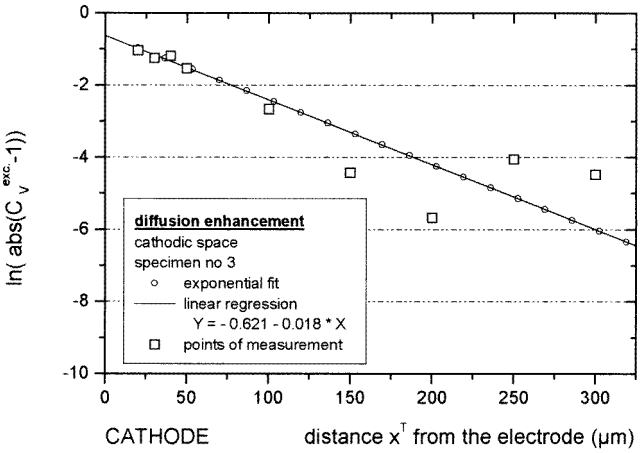

Figure 9. ln[abs($C_V^{exc.} - 1$)] graph versus x^T corresponding to equation (36). The slope of this plot represents the mean square free path of the vacancies of specimen No 3.

the temperature of our reference measurements—which is about four orders of magnitude higher than usual tracer diffusion coefficients at this temperature [7]—one obtains from our experiments vacancy lifetimes of about 42, 89 and 26 s. Differences in the tungsten coating of the front ends of the specimens could have accounted for an asymmetry of the axial copper penetration into the silver rod. This possible effect may had been even enhanced by the electromigration induced different steady-state vacancy concentrations at the front ends of the sample. Since our correction of the diffusion enhancement curves does not consider any asymmetry of axial copper diffusion the scatter of the obtained lifetimes may be due to these effects.

The obtained values of the mean free path and lifetime of the vacancies are in good agreement with theoretical predictions as well as with earlier measurements obtained by thermotransport measurements [6, 8].

5. Summary

The mean free path of excess vacancies that are generated during electromigration in silver rods with current densities between 3500 and 5000 A cm^{-2} has been indirectly measured. The determination of the mean free path values is based on measurements of diffusivities of copper in silver and the assumption that during electromigration locally steady-state concentrations of excess vacancies prevail. The evaluation by means of the derived equations is confined by certain conditions that should be fulfilled in the cases considered here as could be shown *a posteriori*. The measurements are impeded by a boundary diffusion effect that occurs at both ends of the rod-shape specimens. Under the assumption that this effect is independent of the actual electric potentials prevailing at the specimens' ends the results of the measurements could be corrected and evaluated by means of the pertinent equations derived from the premises of the steady-state theory. The mean square free path of the excess vacancies was found to be between 1.6×10^{-4} and 5.4×10^{-4} cm^2. These values correspond to a mean lifetime of excess vacancies between 26 and 89 s, if a vacancy diffusion coefficient $D_V = 1.00 \times 10^{-10}$ m^2 s^{-1} is assumed for a temperature of 943 K as applied in our experiments.

Acknowledgments

The author wishes to express his gratitude to Professor Th Hehenkamp of the Institut für Metallphysik, Universität Göttingen, under whose guidance this work has been carried out. He is also indebted to Professor V Ruth, FB Physik, Universität Oldenburg, for critically reading the manuscript and helping to prepare the English version of this paper.

Appendix A. Solution of the steady-state equation (16)

With the transformation

$$y = C_V^{exc.} - 1 \tag{A1}$$

equation (16) can be rewritten for the linear case considered here as

$$\frac{d^2y}{dx^2} - A\frac{dy}{dx} - By = 0 \tag{A2}$$

with the parameters A and B as defined in equations (15*a*) and (15*b*). The conceivable general premise for a solution

$$y = C_1 e^{r_1 x} + C_2 e^{r_2 x} \tag{A3}$$

is indeed a solution of equation (A2) if the relations

$$r_1^2 - Ar_1 - B = 0 \tag{A4a}$$

$$r_2^2 - Ar_2 - B = 0 \tag{A4b}$$

hold, as can readily be proven by inserting the premise (A3) into the differential equation (A2). From equations (A4*a*) and (A4*b*) follows directly

$$r_{1/2} = \frac{A}{2} \pm \left[\left(\frac{A}{2}\right)^2 + B\right]^{1/2} \tag{A5}$$

which is our relation (19*a*) in the text. With the boundary condition $\boldsymbol{J}_V = \boldsymbol{0}$ being fulfilled at $x = \pm L/2$ (as stated in the text) the coefficients C_1 and C_2 can be determined. If the

boundary condition is not fulfilled, these coefficients have to be replaced by the coefficients C_1' and C_2', as given by equations (20*a*) and (20*b*). For the determinations of C_1 and C_2 the equations (2), (6), (14) and (15*a*) are combined to yield

$$J_V = -D_V C_V^{eq.} \frac{\mathrm{d}C_V^{exc.}}{\mathrm{d}x} + D_V C_V^{eq.} A C_V^{exc.}. \tag{A6}$$

With the boundary condition applied to this equation one obtains with the solution (A3) the relations (19*b*) and (19*c*).

Appendix B. The condition (27) and that for $J_V = 0$ at the specimen's ends

The electric field E can easily be related to the measured current density I:

$$\frac{EL}{Ia} = \frac{U}{\mathcal{J}} = R = \rho \frac{L}{a} \tag{B1}$$

with the length and the cross-sectional area of the specimen L and a and the standard definitions of voltage U, current $\mathcal{J}$, resistance R and the specific resistance ρ.
From (B1) follows

$$E = \rho I. \tag{B2}$$

With a specific resistance of silver at 943 K of $\rho_{943} \cong 5.45 \times 10^{-6}$ V cm A^{-1} and a measured current density of $I \cong 4.5 \times 10^3$ A cm^{-2} one obtains for our experiments according to equation (15*a*)

$$\frac{A}{2} \cong 0.15 Z^* \text{ cm}^{-1} \tag{B3}$$

whereas we obtain for $B^{1/2}$ according to relation (15*b*) with a measured diffusivity of a vacancy $D_V = 1.00 \times 10^{-10}$ m^2 s^{-1} and from our measurements for the lifetime of an excess vacancy $\tau_V \leqslant 1000$ s a value exceeding 33.6 cm^{-1}. Even for an estimated effective valence of a vacancy $Z^* \cong 10$ one notes that the condition (27) is fulfilled. Hence, the weaker condition (23) is expected to be fulfilled in any case.

According to the definitions of the parameters A'_{cat} and A'_{an}, equations (21*a*) and (21*b*), these parameters can be approximated by the parameter A, defined by equation (15), if the condition

$$J_V^{an,\,cat} \ll \frac{Z^* e E}{kT} D_V C_V^{eq} \tag{B4}$$

is fulfilled. With the estimated value of $A \cong 3 \times 10^2$ m^{-1}, an assumed diffusivity of a vacancy, $D_V = 1.00 \times 10^{-10}$ m^2 s^{-1}, and an equilibrium vacancy concentration of about $10^{-4} C_s$—where $C_s = 5.9 \times 10^{28}$ m^{-3} is the number of lattice sites per unit volume in a lattice crystal—condition (B4) is fulfilled if $J_V^{an,\,cat} \ll 1.8 \times 10^{17}$ m^{-2} s^{-1}.

References

[1] Hehenkamp Th 1993 *Non Equilibrium Concentration of Vacancies During Atomic Transport, Defect and Diffusion Forum* **95–98** 171
[2] Barreau G, Brunel G, Zizeron G and Lacombe P 1971 *Mem. Sci. Rev. Metall.* **68** 357
[3] Dorner P, Gust W, Hintz M B, Lodding A, Odelius H and Predel B 1979 *Acta Metall.* **28** 291
[4] Sawatzki A and Jaumot F E 1957 *Trans. AIME* **209** 1207
[5] Hall M G and Haworth C W 1970 *Diffusion Data* Vol 4, 10 [A93]
[6] Rödel Th 1989 *Dissertation* Universität Göttingen
[7] Mosig K, Wolff J, Kluin J E and Hehenkamp Th 1992 *J. Phys.: Condens. Matter* **4** 1447
[8] Kossak R 1985 *Dissertation* Universität Göttingen